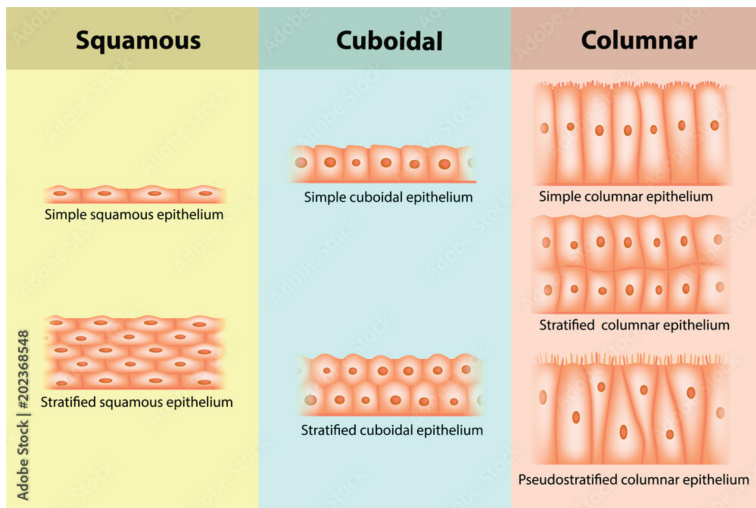


# Chapter 2

## Vertex models of tissues

Epithelia form one of the four basic animal tissue along with connective, muscle and nervous tissues and are omnipresent in animal organs. It generally consists in a thin continuous and tightly compacted layer of cells, which forms the outer or inner layer of many organs and cavities, such as the epidermis in the skin. Epithelial tissues can be formed of a single layer or by two or more stratified cell layers, where cells generally adopt three major types of shapes in 3 dimensions: squamous, columnar and cuboidal (see Fig 2.1f). In this chapter, we will focus on epithelial monolayers from a mechanical perspective, through the lens of so-called *vertex models*, which are discrete and simple models of cell shape and mechanics parametrized by vertices.



**Figure 2.1:** The three main types of epithelial cell organization: squamous, cuboidal and columnar. The epithelial tissue can be made of a monolayer or by several stratified (or pseudo-stratified) layers of cells.

### 2.1 2D vertex models of epithelial tissues

The figure 2.2 shows a monolayer epithelium, the wing of the drosophila, imaged from above (*apical* surface) using a confocal microscope, with fluorescently labeled cell membranes. Cells in monolayers adopt very commonly regular polygonal shapes, which motivates their discrete modeling as polygons in 2D or polyhedra in 3D. In Fig. 2.3, we show that the polygonal organization of epithelial monolayer does not depend on the tissue type (wing vs. notum of the Drosophila), and we illustrate the 3D structure of an epithelium with a side-view of a suspended monolayer of MDCK cells [1].

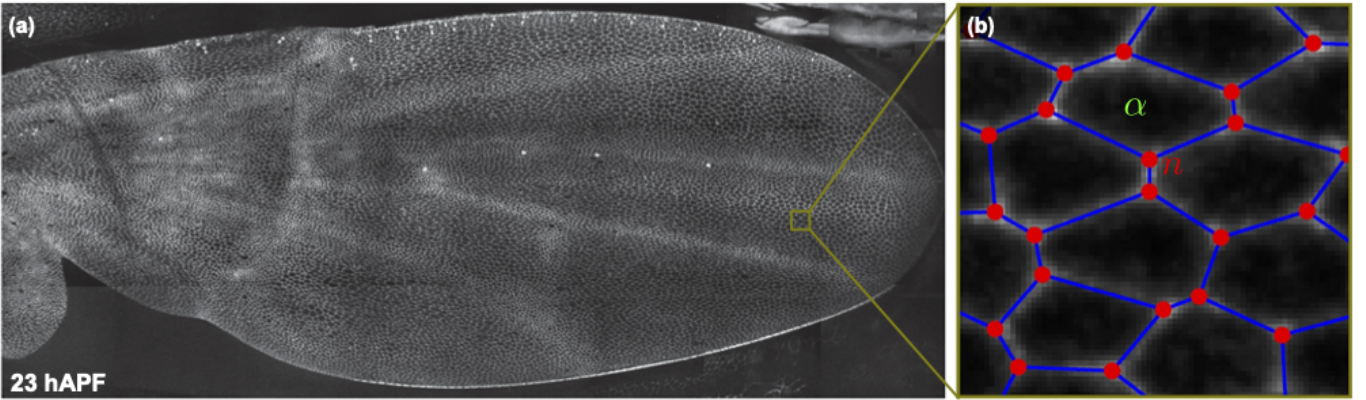


**Figure 2.2:** Microscopy image of a Drosophila wing and corresponding 2D polygonal representation [2]

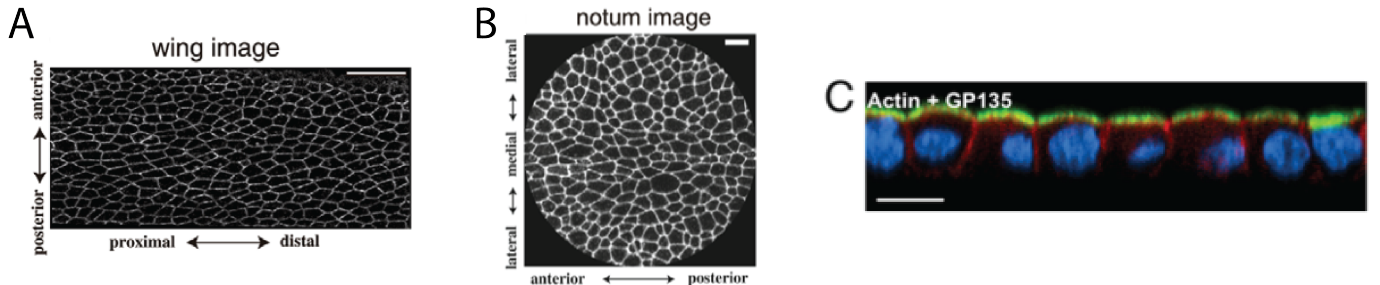


**Figure 2.3:** Microscopy images of a piece of the Drosophila wing (A), of the Drosophila notum (B) [3] and side-view of a suspended monolayer of MDCK cells [1]

### 2.1.1 Topology

#### Euler relation

We first establish a few mathematical relations for a surface paved by polygons. This paving is modeled

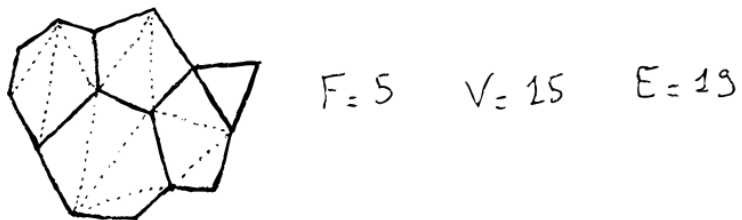


**Figure 2.4**

as a graph of  $F$  polygons (or faces),  $V$  vertices and  $E$  edges. On the example below on Fig. 2.4, we have specifically  $F = 5$ ,  $V = 15$  and  $E = 19$ . Euler found a topological relationship between these numbers

$$F + V - E = 1 \quad (2.1)$$

The demonstration may be done graphically: by adding an edge in a polygon (dashed lines on Fig. 2.4) to form a triangle, one doesn't change  $F + V - E$  because one adds one edge and one face. Doing so, one can replace the polygonal paving into a triangular mesh, keeping  $F + V - E$  constant. Similarly, if one triangle at the border of the paving is removed,  $F + V - E$  remains constant. At the end, one has one triangle left, for which the relation  $F + V - E = 1$  becomes obvious.

#### Topological transitions

In 2D epithelial tissues, we generally find only 3-fold junctions: each vertex has exactly 3 edges. This

property is well known in foams, where 4-fold junctions or junctions of higher degrees are unstable and will spontaneously evolve toward 3-fold junctions. This topological transition is generally called a T1-transition, which is schematized on Fig. 2.5. Another classical topological transition happening in epithelial tissues is the T2-transition, which corresponds to the disparition of a cell (because of cell death or cell extrusion) and reformation of a new 3-fold junction instead.

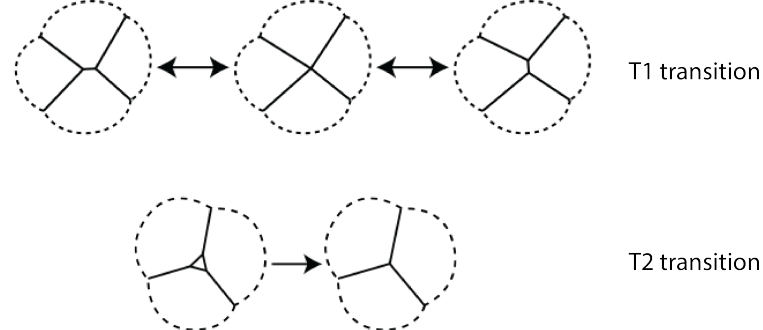


**Figure 2.5:** T1 and T2 topological transitions

### Hexagonal packing

Epithelial tissues adopt often cell packing which are close to hexagonal networks. This fact may be understood through a simple mean-field argument. Because of the presence of 3-fold junctions only, the number of vertices and edges are related to each others as follows  $3V = 2E$ . The mean number of edges in a polygon is  $\langle n \rangle \equiv \frac{2E}{F} = \frac{3V}{F}$  (each edge is shared between 2 polygons). From the Euler relation, we have furthermore  $1 + \frac{V}{F} - \frac{E}{F} = \frac{1}{F}$ , which leads to  $\langle n \rangle (\frac{1}{3} - \frac{1}{2}) + 1 = \frac{1}{F}$ . Taking the limit of a large tissue  $F \rightarrow +\infty$ , we obtain therefore  $\langle n \rangle = 6$ .

The mean polygon for large tissues is therefore akin a to an hexagon with 6 edges. If there exists polygons of less than 6 edges, then the tissue will also necessarily have polygons of more than 6 edges as well.

#### 2.1.2 2D vertex model

The cell elasticity is dominated by the cortical contractility, but different interfaces and junctions may have different contributions to tension. Lateral surfaces (cell-cell contact) are the sum of adhesive and cortical contributions. The apical and basal (which adheres to the basement membrane) surfaces are both under tension, but each the apical side is furthermore equipped with an actomyosin belt, which follows cell junctions and is highly contractile, creating an additional line tension. We will describe the mechanics of the epithelial tissue using a polygonal paving of its apical surface. The contribution of lateral surface and basal surface are essentially neglected (see Fig 2.6). In 2-dimensions, the cell elasticity depends on the face and tensions are line tensions located at edges.

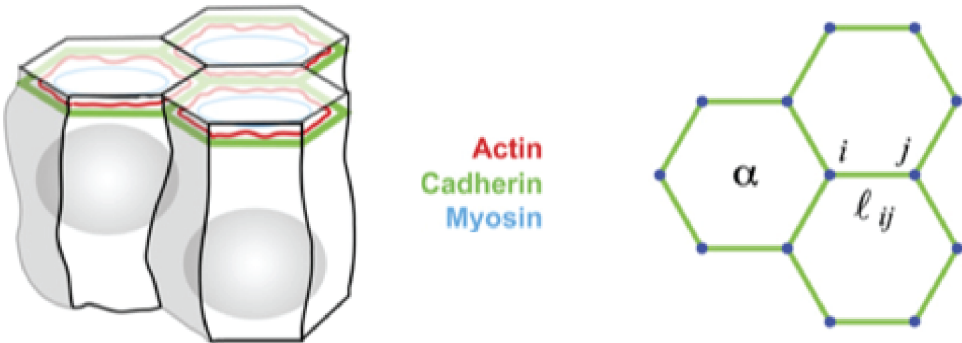


**Figure 2.6:** Schematics of the epithelium and corresponding 2D vertex model

Following the notations in the original publication [4], each cell is defined by an index  $\alpha$ , each vertex by an index  $i$  and each edge by a pair of indices  $< i, j >$ . The force may be derived from an effective energy that reads

$$\mathcal{E} = \sum_{\alpha} \frac{\kappa_{\alpha}}{2} (A_{\alpha} - A_{\alpha}^0)^2 + \sum_{<i,j>} \Lambda_{ij} \ell_{ij} + \frac{1}{2} \sum_{\alpha} \Gamma_{\alpha} P_{\alpha}^2 \quad (2.2)$$

The first term supposes that for each cell  $\alpha$  there is a surface elasticity associated to the constant  $\kappa_{\alpha}$ , which tends to bring the current area  $A_{\alpha}$  back to its preferred value  $A_{\alpha}^0$ . This term is associated to the apical tension, but may also somehow account for the effective elastic response of a cell in 3D, which has a preferred shape dictated by apical, basal and lateral tensions and the constraint of volume conservation.

$\Lambda_{ij}$  is the (line) tension associated to an edge  $< i, j >$  and the last term accounts for the possible variation of tension with the cell shape, here via the square of its perimeter  $P_{\alpha}$ . The effective tension will be different at each edge because of this term.

### Ground states of a single cell

Here we follow in particular [5]. In the next, we suppose an homogeneous tissue, such that  $\kappa_{\alpha} = \kappa$ ,  $\Lambda_{ij} = \Lambda$  and  $\Gamma_{\alpha} = \Gamma$ . The tissue energy reduces then to a simple sum on each cell

$$\mathcal{E} = \sum_{\alpha} \frac{\kappa}{2} (A_{\alpha} - A_0)^2 + \frac{\Lambda}{2} P_{\alpha} + \frac{\Gamma}{2} P_{\alpha}^2 \quad (2.3)$$

The energy is renormalized to work with dimensionless parameters. We choose as characteristic length in the tissue  $\sqrt{A_0}$ , such that  $A_{\alpha} = A_0 a_{\alpha}$ ,  $P_{\alpha} = \sqrt{A_0} p$ , and we define  $\bar{\Lambda} = \frac{\Lambda}{\kappa A_0^{3/2}}$ ,  $\bar{\Gamma} = \frac{\Gamma}{A_0 \kappa}$ ,  $p_0 = -\frac{\Lambda}{2\Gamma}$  and  $e_0 = -\frac{\bar{\Lambda}^2}{8\Gamma}$ , such that the dimensionless energy reads

$$\bar{\mathcal{E}} \equiv \frac{\mathcal{E}}{\kappa A_0^2} = \sum_{\alpha} \left\{ \frac{(a_{\alpha} - 1)^2}{2} + \frac{\bar{\Gamma}}{2} (p_{\alpha} - p_0)^2 + e_0 \right\} \quad (2.4)$$

The system is therefore controlled by 3 dimensionless parameters  $\bar{\Gamma}$ ,  $p_0$  and  $e_0$ .

We first study the configuration of a single, cell. Its dimensionless energy is simply  $e = \frac{1}{2}(a - 1)^2 + \frac{\bar{\Gamma}}{2}(p - p_0)^2 + e_0$ . Dilating the cell by a factor  $\alpha$ , we obtain

$$e(\alpha) = \frac{1}{2} (\alpha^2 a - 1)^2 + \frac{\bar{\Gamma}}{2} (\alpha p - p_0)^2 + e_0$$

The energy is minimal for a non-dilated cell if and only if  $\frac{\partial e}{\partial \alpha} \Big|_{\alpha=1} = 0$ , which gives

$$2a(a - 1) + \bar{\Gamma}p(p - p_0) = 0 \quad (2.5)$$

One can distinguish four possible cases:

- **$a = 1$  and  $p = p_0$** : this is the absolute minimum of the energy  $e = e_0$ , at which both area and perimeter take their preferred values. More details are given below
- **$a > 1$  and  $p < p_0$** : such cell is unstable with respect to shear, because  $\frac{\partial e}{\partial p} \Big|_a = \bar{\Gamma}(p - p_0) < 0$  and it is always possible to decrease the energy by increasing the perimeter at fixed area.
- **$a < 1$  and  $p > p_0$**  such cell is stable with respect to shear, because  $\frac{\partial e}{\partial p} \Big|_a = \bar{\Gamma}(p - p_0) > 0$ , so at fixed area, one can decrease the energy by lowering the perimeter.

- $a = 0$  and  $p = 0$ : this is a collapsed cell, for which the energy is  $e_c = e_0 + \frac{\bar{\Gamma}}{2} p_0^2 + \frac{1}{2} = \frac{1}{2}$ .

**The case  $a = 1$  and  $p = p_0$**  gives an absolute minimum of the energy but it can be accessed only for certain values of the perimeter  $p_0$ . For an area  $a = 1$ , the minimal perimeter is the one of a regular polygon with  $n$  sides<sup>1</sup>:  $p_0 = -\frac{\bar{\Lambda}}{2\bar{\Gamma}} \geq (4n \tan \frac{\pi}{n})^{\frac{1}{2}}$ , which gives

$$\bar{\Lambda} \leq \bar{\Lambda}_n \equiv -4\bar{\Gamma} \left( n \tan \frac{\pi}{n} \right)^{1/2} \quad (2.6)$$

For  $n = 3, 4, 5, 6, \dots$ , we can therefore define threshold values of  $\bar{\Lambda}$  such that  $\bar{\Lambda}_3 < \bar{\Lambda}_4 < \bar{\Lambda}_5 < \bar{\Lambda}_6 = -\bar{\Gamma} 2^{5/2} 3^{1/4} \dots < -4\bar{\Gamma}$ , such that if  $\bar{\Lambda} > \bar{\Lambda}_n$ , only polygons of more than  $n$  sides (strictly) are at a minimum of energy. For instance, for  $\bar{\Lambda} \geq \bar{\Lambda}_5$ , the (absolute) minimum is reached for (irregular) hexagons and polygons of more than 6 sides.

**The case  $a < 1$  and  $p > p_0$** : if  $p > p_0$ , at fixed area, one can decrease the energy by lowering the perimeter. This case always leads either to regular polygons or a collapsed cell ( $a = 0, p = 0$ ). A regular polygon has a smaller perimeter than any irregular  $n$ -sided polygon with the same area. Thus if  $p > 0$ , the optimal cell shape is a regular  $n$ -sided polygon. For a regular polygon, the area is given by  $a = \frac{\cot(\pi/n)}{4n} p^2 \equiv c_n p^2$ . The minimum of the energy is obtained for this regular polygon if the condition Eq. 2.5 is verified, which gives

$$2c_n p^2 (c_n p^2 - 1) + \bar{\Gamma} p(p - p_0) = 2c_n p^2 (c_n p^2 - 1) + \bar{\Gamma} p^2 + \bar{\Lambda} p = 0 \quad (2.7)$$

This minimum is locally stable if and only if its energy is less than the one of a collapsed cell  $e(p) \leq \frac{1}{2}$ .

A necessary condition for polygonal collapse is given by  $e(p) > \frac{1}{2}$ , which combined with the equation for stability Eq. 2.7 determines the transition through the two quantities  $\bar{\Gamma}$  and  $p$  and leads to two cases [5]

- If  $\bar{\Gamma} \geq 2c_n$ , the only solution is  $p = \bar{\Lambda} = 0$ , which corresponds to a collapsed cell.
- If  $\bar{\Gamma} < 2c_n$ , the collapse it attained for  $\bar{\Lambda} > \bar{\Lambda}_c = \frac{2}{c} \left( \frac{2c-\bar{\Gamma}}{3} \right)^{3/2}$  where  $p = \frac{3}{c_n} (2c_n - \bar{\Gamma})^{1/2}$ .

For hexagons, for which  $c_6 = \frac{1}{8\sqrt{3}}$ . If  $\bar{\Lambda} = \bar{\Lambda}_6 = -2^{5/2} 3^{1/4} \bar{\Gamma}$ , the equation (2.7) is verified for  $a = 1$  and  $p = 3^{1/4} 2^{3/2}$ . If  $\bar{\Lambda} > \bar{\Lambda}_6$  at  $\bar{\Gamma}$  fixed, then the area and perimeter of hexagons is decreasing with  $\bar{\Lambda}$ . This can lead to collapsed cells (unstable tissue) and regular hexagons of area less than 1. The transition to collapse from hexagonal cells is therefore given by the two cases (as summarized in the Table Fig.2.8A):

- If  $\bar{\Gamma} \geq \frac{\sqrt{3}}{12}$ , the only solution is  $p = \bar{\Lambda} = 0$ , which corresponds to a collapsed cell.
- If  $\bar{\Gamma} < \frac{\sqrt{3}}{12}$ , the collapse it attained for  $\bar{\Lambda} > \bar{\Lambda}_c = 2 \cdot 3^{-5/2} (\sqrt{3} - 12\bar{\Gamma})^{3/2}$

## Ground states of a single cell

Numerically, Staple et al. [5] are recovering for a tissue a certain number of the theoretical results obtained for a cell above and a few new configurations that combine several cell topologies.

As shown on Fig. 2.8B for  $\bar{\Lambda} \leq \bar{\Lambda}_6$  (solid line), the tissue adopts a fundamental state, where the energy is at the absolute minimum ( $a = 1$  and  $p = p_0$ ), but where there exists many degenerate cases with irregular polygons of with more than 3 sides, that corresponding to soft modes of deformation (i.e. modes of deformations of the tissue that do not cost any energy). The degeneracy decreases as  $\bar{\Lambda} \geq \bar{\Lambda}_n$  with  $3 \geq n \geq 6$ , as the  $n$ -sided polygons become impossible. Above  $\bar{\Lambda}_6$ , only polygons of more than 6 sides could be in the fundamental state, but that would not yield the mean side number  $\langle n \rangle = 6$  predicted above. Therefore, the tissue adopts rather a regular and periodic hexagonal pattern, which does not correspond to the absolute

---

<sup>1</sup>For a regular polygon of degree  $n$ , we have  $\tan \frac{\pi}{n} = \frac{\ell}{h}$ , where  $\ell$  is the side length and  $h$  the apothem (shortest distance from the center to one side). We deduce the area  $a = n(h \frac{\ell}{2}) = n \frac{\ell^2}{4} (\tan \frac{\pi}{n})^{-1}$ , and the perimeter  $p = n\ell = (4an \tan \frac{\pi}{n})^{1/2}$  as function of the area.

A

Parameter values		Ground state (identical cells)
$\bar{\Lambda} < -2^{5/2}3^{1/4}\bar{\Gamma}$	-	irregular polygons ( $a = 1, p = p_0$ )
$-2^{5/2}3^{1/4}\bar{\Gamma} \leq \bar{\Lambda} < 2 \cdot 3^{-5/2}(\sqrt{3} - 12\bar{\Gamma})^{3/2}$	$\bar{\Gamma} < \sqrt{3}/12$	hexagonal lattice }
$-2^{5/2}3^{1/4}\bar{\Gamma} \leq \bar{\Lambda} < 0$	$\bar{\Gamma} \geq \sqrt{3}/12$	
$\bar{\Lambda} \geq 2 \cdot 3^{-5/2}(\sqrt{3} - 12\bar{\Gamma})^{3/2}$	$\bar{\Gamma} < \sqrt{3}/12$	collapsed lattice ( $a = 0, p = 0$ ) }
$\bar{\Lambda} \geq 0$	$\bar{\Gamma} \geq \sqrt{3}/12$	

B

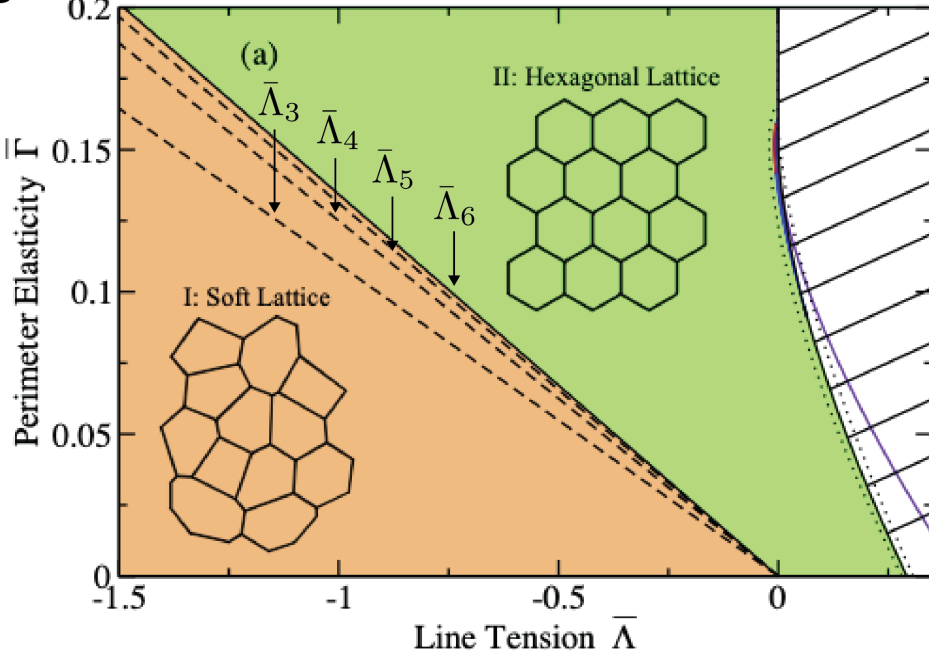


**Figure 2.7: Ground state for the 2D vertex model [5].** (A) Table of the different transition boundaries between the different ground states depending on  $\bar{\Lambda}$  and  $\bar{\Gamma}$ . (B) Numerical phase diagram of the ground state for the 2D vertex model as function of  $\bar{\Gamma}$  and  $\bar{\Lambda}$  with the corresponding transition boundaries predicted theoretically.

minimal state of energy  $\mathcal{E} = N_{\text{cell}}e_0$ . The new fundamental state corresponds to hexagons with  $a < 1$  and  $p > p_0$ . This structure remains stable if cells don't collapse. The conditions of collapse were predicted for a single cell above for the particular case of an hexagon, and are reported in the Table Fig. 2.8A.

Numerically, the authors find that the regular hexagonal pattern is the only fundamental state for  $\bar{\Lambda} \geq \bar{\Lambda}_6$ , except for two very small regions depicted in more details on Fig. ???. Two regions with two different types of cells organized in a periodic manner can have a lower energy than the hexagonal arrangement and are represented in red and blue.

### Comparison to experiments

In Farhadifar et al. [4], the authors compare the shape properties of the 2D vertex model with the cell packing observed in imaginal disk of the Drosophila wing. The authors add growth and division (proliferation) and allow for topological transitions (T1 and T2 transitions, see Fig. 2.5 and study the statistical properties of stationnary states. They systematically vary  $\bar{\Gamma}$  and  $\bar{\Lambda}$  to get the best fit to measured values of the distribution of polygons and their mean area (see Fig. 2.9. They also use laser ablation experiments to directly compare the relative area and bon length change depending on the values of  $\bar{\Gamma}$  and  $\bar{\Lambda}$ .

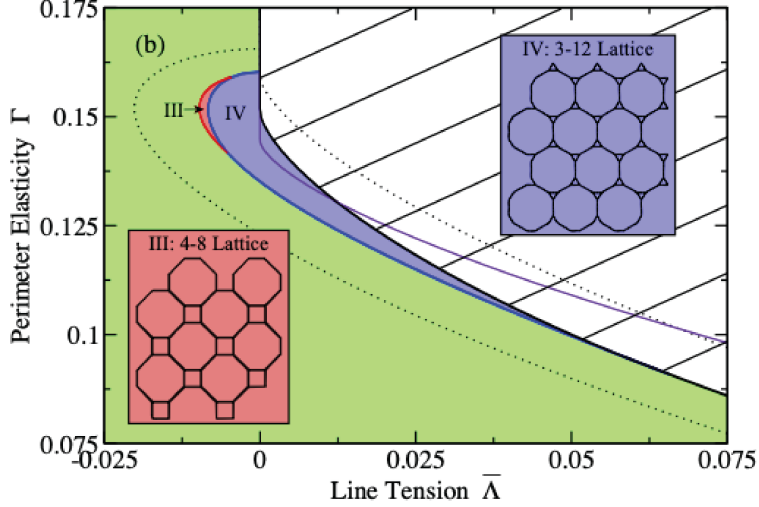


**Figure 2.8: Ground state for the 2D vertex model - Possible non-hexagonal patterns with two cell types for  $\bar{\Lambda} \geq \bar{\Lambda}_6$  [5].**

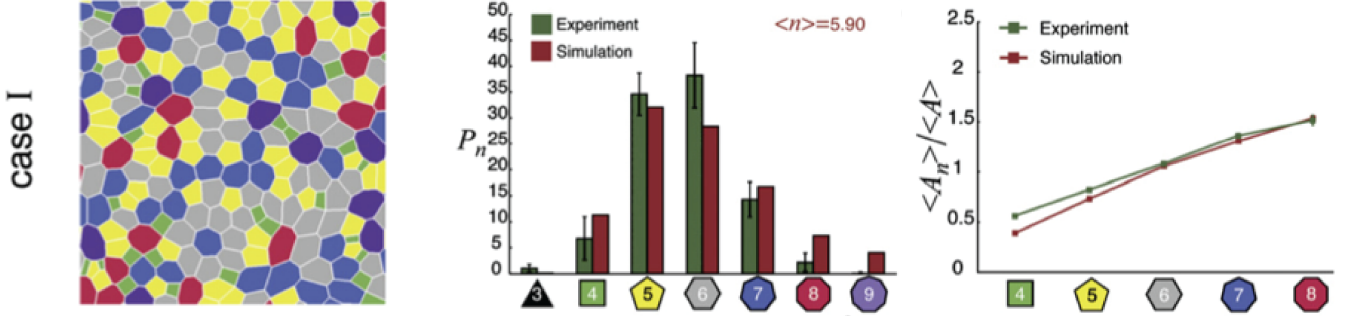


**Figure 2.9: Schematics of the epithelium and corresponding 2D vertex model [4].**

## 2.2 3D vertex models

To better account for the 3D structure of cells, several 3D vertex models have been proposed in the last decades, relying mostly on numerical implementations. Here we will focus on a model that was proposed by Hannezo et al. [6], because it remains relatively easy to describe analytically.

### 2.2.1 Epithelial 3D vertex model (Hannezo et al. 2014)

To simplify we consider a monolayer of cells, that are all **identical**, and whose **apical surface remains hexagonal**. The basal surface has therefore also an hexagonal geometry and lateral surfaces are parallelograms. We note  $h$  the height of a cell and  $r$  the radius of the circle circumscribed to the hexagon. A cell is defined as columnar when  $\frac{h}{r} \gg 1$ , squamous when  $\frac{h}{r} \ll 1$  and cuboidal when  $\frac{h}{r} \sim 1$ .

The apical area is  $A_a = r^2 \frac{3^{3/2}}{2}$ , and the total lateral surface area is  $A_L = 6rh$ . The volume of the cell is simply  $V = Ah$ .

Exactly like for the 2D vertex model, we write an energy that accounts for the tensions (and adhesion) at each interface, the minimization of which defining the mechanical equilibrium. For a single cell it reads

$$e = \gamma_L A_L + \gamma_b A_b + \gamma_a A_a + \Lambda P + \frac{K}{2} \frac{(V - V_0)^2}{V_0} \quad (2.8)$$

where  $\gamma_L$ ,  $\gamma_a$ ,  $\gamma_b$  are surface tensions of respectively the lateral, apical and basal surfaces,  $\Lambda$  is the apical line tension, multiplied by the apical perimeter  $P$  and  $K$  measures the cell compressibility, which shall bring the

volume  $V$  of the cell back to its target value  $V_0$ . This compression modulus is supposed high in the next, such that  $V \sim V_0$ .  $\gamma_L, \gamma_a, \gamma_b$  have a positive contribution from the actomyosin contractility, but  $\gamma_L$  and  $\gamma_b$  also have a negative contribution coming from cell-cell adhesion for lateral surfaces and from the adhesion to the basal membrane for the basal surface. In principle, they may therefore become negative as well.

### Flat epithelial monolayers

In the next, to simplify we define  $\gamma = \gamma_a + \gamma_b$ , as the monolayer is supposed to remain flat in this paragraph. We further ignore numerical prefactors, which simply renormalize the tensions. The energy for a cell reads then simply

$$e = \gamma r^2 + \Lambda r + \gamma_L \frac{V_0}{r} \quad (2.9)$$

where we have used the constraint of volume conservation to express  $h = \frac{V_0}{A} \sim \frac{V_0}{r^2}$ .

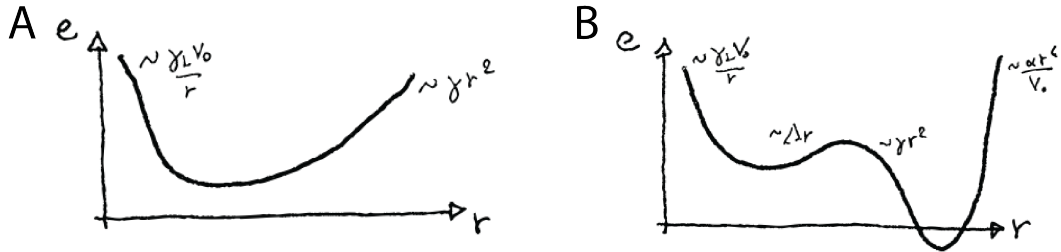


**Figure 2.10:** Sketch of the plot of the cell energy for a flat 3D vertex model (A) If  $\gamma > 0$ , there is a single minimum. (B) if  $\gamma < 0$ , there can be two minima, adding a limit to compressibility with a new term  $\frac{\alpha}{h^2} \sim \frac{\alpha r^4}{V_0}$ .

If  $\gamma > 0$ , there is a single minimum of the energy, given by the derivative of  $e$  with  $r$ :

$$2\gamma r + \Lambda - \gamma_L \frac{V_0}{r^2}$$

We sketch the plot of the energy on Fig. 2.10A and we can distinguish two limit cases

- If  $\Lambda$  is high enough, then  $r$  will be small and the equation above reduces to  $\Lambda - \gamma_L \frac{V_0}{r^2} \sim 0$ , which gives  $r = \left(\frac{V_0 \gamma_L}{\Lambda}\right)^{1/2}$  and  $h = \frac{\Lambda}{\gamma_L}$ .
- If  $\Lambda$  is small enough, then it is negligible and the equation above reduces to  $2\gamma r^2 - \gamma_L \frac{V_0}{r^2} = 0$ , which leads to  $r = \left(\frac{\gamma_L V_0}{2\gamma}\right)^{1/3}$

One can see that  $r$  increases if  $\gamma$  and/or  $\Lambda$  decreases and if  $\gamma_L$  increases: we switch continuously from columnar cells (very elongated vertically) to squamous cells (very flat).

If  $\gamma < 0$ , the energy may be non-monotonous as sketched on Fig. 2.10B. The absolute minimum is for  $r \rightarrow +\infty$ , but the cell cannot collapse fully because there is incompressible material within. To account for this effect, a new term is added to the energy in the form  $e_{\text{com}} = \frac{\alpha}{h^2} \sim \frac{\alpha r^4}{V_0}$ . This creates a second possible minimum, with a possible discontinuous transition between the two minima<sup>2</sup>.

<sup>2</sup>By adding this additional term, one can write the energy for a cell  $e = \gamma A + \frac{\alpha}{V_0^2} A^2 + (\Lambda + \gamma_L h) P$ . If one considers  $\Lambda$  much larger than  $\gamma_L h$ , which means that we ignore the lateral tension, we recover almost the expression used by Farhadifar's et al [4] for the 2D vertex model. The term  $\frac{\alpha P^2}{2}$ , which comes from the variation of the tension with the perimeter  $P$  is however missing.

## Tissue under tension

The tension of the tissue may be defined as the derivative of the energy with respect to the area. At the level of a single cell, it reads therefore

$$\Gamma = \frac{\partial e}{\partial A} = \frac{1}{2r} \frac{\partial e}{\partial r} = \gamma + \frac{\Lambda}{2r} - \frac{\gamma_L V_0}{2r^3} \quad (2.10)$$

At mechanical equilibrium, (no tension) we should have  $\Gamma = 0$ . The plot of the tissue tension is sketched on Fig. 2.11

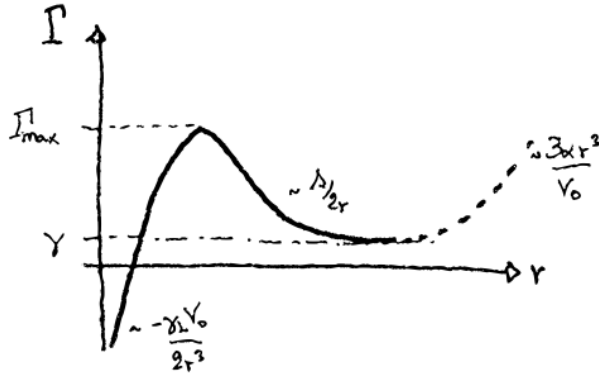


**Figure 2.11: Sketch of the plot of the tissue tension for a flat 3D vertex model.** The dotted line is the continuation of the tissue tension if the term  $\frac{\alpha}{h^2} \sim \frac{\alpha r^4}{V_0}$  is added to the energy.

We see that the tension reaches a maximum  $\Gamma_{\max} = \gamma_L + \frac{\Lambda^{3/2}}{2\sqrt{3}\gamma_L V_0} \left(1 - \frac{\gamma_L}{6}\right)$ , which is obtained for  $r = \left(\frac{2\gamma_L V_0}{\Lambda}\right)^{1/2}$ . As  $r \rightarrow +\infty$ , the tissue tension approaches  $\gamma_L$ .

For  $\Gamma > \Gamma_{\max}$  then the tissue is unstable and there is no solution other than  $h \rightarrow 0$ , unless the additional term  $\frac{\alpha}{h^2} \sim \frac{\alpha r^4}{V_0}$  is added. In the case of a discontinuous transition  $\gamma < 0$ , the tissue tension transforms columnar cells into cuboidal or squamous cells.

### 2.2.2 Non-epithelial 3D vertex models

#### 3D polyhedral models

In fact, the first 3D vertex models were proposed by Honda et al. [7]. In this paper, the authors study the flattening of a small aggregate made of polyhedral cells under the action of a centrifugal volume force. In this model, there is still a geometric constraint on cells, which are supposed to have flat interfaces, neglecting hence Laplace's pressure.

The total energy of the system is defined as

$$\mathcal{E} = \sigma \sum_{<\alpha, \beta>} A_{\alpha\beta} + \sigma_0 \sum_{<\alpha, 0>} A_{\alpha 0} + \kappa \sum_{\alpha} (V_{\alpha} - V_0)^2 + \rho \sum_{\alpha} z_{\alpha} V_{\alpha} + w_{\text{floor}} \sum_{\alpha} \frac{1}{1 + e^{az_{\alpha}}} \quad (2.11)$$

The first two terms account for the surface tension of cell-cell and cell-medium interfaces. The second term measures the compressibility of each cell, such that if  $\kappa$  is high, the volume  $V_{\alpha}$  will stay close to its target value  $V_0$ . The two last terms account for the centrifugal force, which creates a potential proportional to the cell height  $z_{\alpha}$  and for the repulsion energy from the floor, which is maximum and equal to  $w_{\text{floor}}$  for  $z_{\alpha} = 0$ .

The deformation of the aggregate is solved by supposing a friction  $\eta$  on each vertex and by solving the overdamped equation balancing on each vertex  $i$  this friction force and the forces derived from the above

energy

$$\eta \frac{d\mathbf{r}_i}{dt} = -\nabla_i \mathcal{E} \quad (2.12)$$

The authors account for both T1 and T2 transitions in the vertex dynamics and obtain numerical results as shown on Fig.2.13

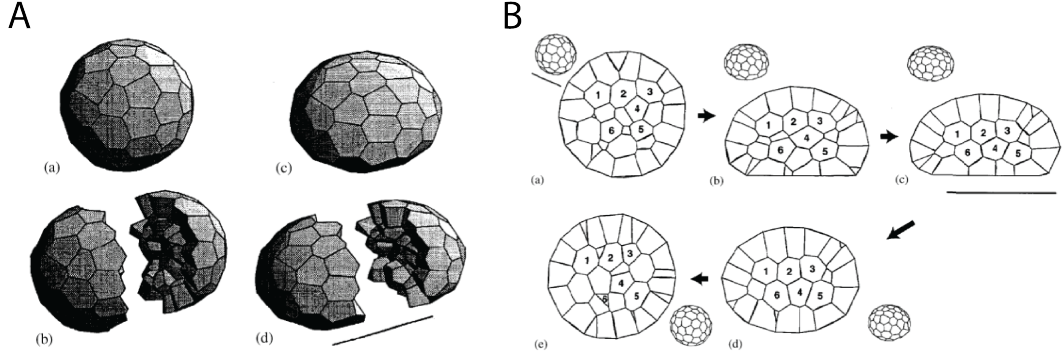


**Figure 2.12: 3D polyhedral models of a cell aggregate [7].** (A) Cell aggregate modeled with polyhedral cells. (B) Section showing cell rearrangements during the flattening and recovery of the aggregate.

More recently, this approach was generalized by Okuda et al. [8], to integrate coupling between mechanics and signalling. Turing equations are solved at the multicellular scale, accounting for the transport of activator and inhibitor molecules across cells via a parameter  $\chi$ , and proliferation is coupled to the activator level. Depending on parameters, this mechanochemical model can lead to various self-organized shape emergence, with budding, branching and tubulation as illustrated on Fig.2.14.

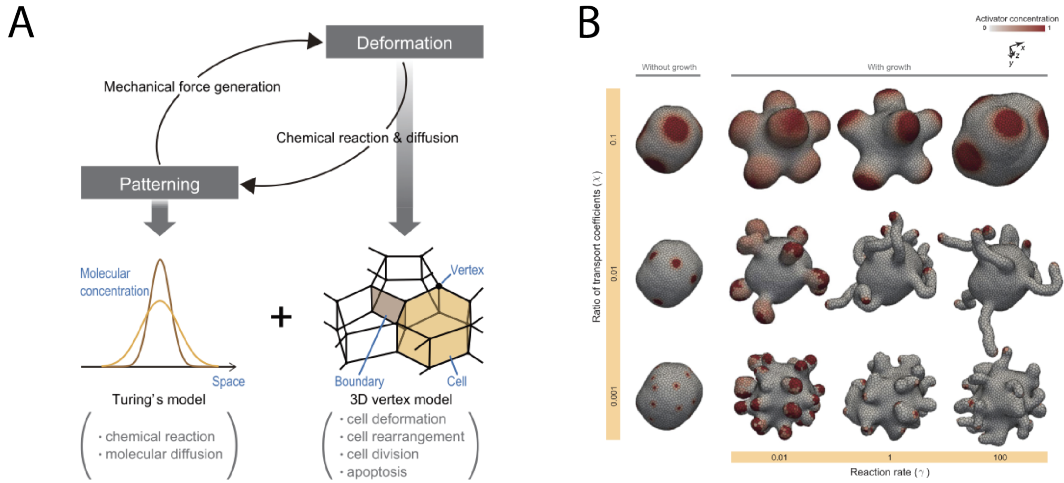


**Figure 2.13: 3D mechanochemical vertex model [8].** (A) Principle of the coupling between cell mechanics and signalling. (B) Examples of self-organized shape emergence depending on a transport coefficient  $\chi$  for the activator between cells, and the reaction rate  $\gamma$ .

### Generic 3D curved vertex model

We now present a generic 3D vertex model, where the cell interfaces are not supposed flat anymore. This requires the parametrization of cell interfaces with a (triangular) mesh, as developed in [9].

**Surface energy and Lagrangian function** The surface energy for a set of  $N$  cells is defined as follows

$$\mathcal{E} = \sum_{\langle l,m \rangle} \gamma_{lm} A_{lm} \quad (2.13)$$

where  $\gamma_{lm}$  and  $A_{lm}$  are respectively the surface tension and area of the interface between regions  $l$  and  $m$  that span  $\llbracket 0, N \rrbracket$ . To account for volume conservation, we define a Lagrangian function from this energy, where  $p_l$  are the Lagrange multipliers (pressures) associated to the volumes  $V_l$

$$\mathcal{L} = \mathcal{E} - \sum_{\text{cell } l \in \llbracket 1, N \rrbracket} p_l (V_l - V_l^0) \quad (2.14)$$

where  $V_l^0$  is the target volume value of the cell  $l$ . Note that for interfaces  $l$  and  $m$  span  $\llbracket 0, N \rrbracket$ , where 0 refers to the external medium, while for cells  $l$  spans  $\llbracket 1, N \rrbracket$ .

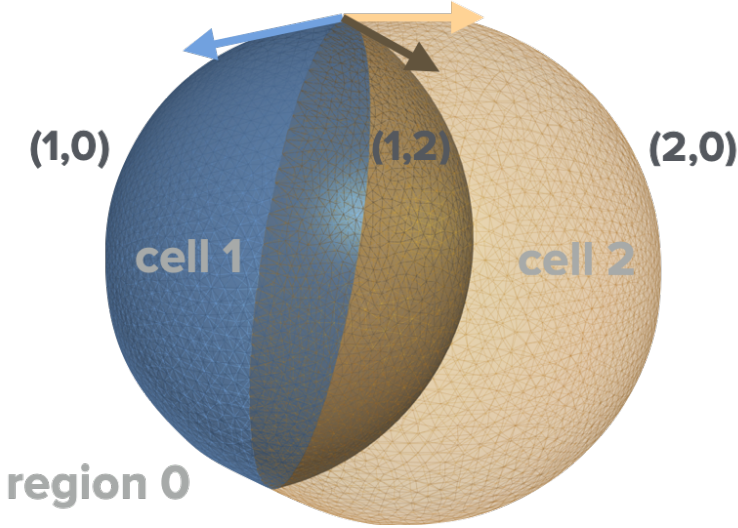


**Figure 2.14: 3D curved vertex model [9].** The cells geometry is parametrized with a non-manifold triangular mesh, where each holds a doublet of integers to keep track of the regions (or cells) between which they lie.

From the Lagrangian function, one can calculate the force  $\mathbf{f}_k$  on each vertex of the mesh  $\mathbf{x} \in \{\mathbf{x}_k\}_{k=1}^n$  as follows

$$\mathbf{f} = -\frac{\partial \mathcal{L}}{\partial \mathbf{x}} \quad (2.15)$$

where  $\mathbf{x} = x\mathbf{e}_x + y\mathbf{e}_y + z\mathbf{e}_z$  and  $\mathbf{f}_k = f^x\mathbf{e}_x + f^y\mathbf{e}_y + f^z\mathbf{e}_z$  are the decomposition of vertex position and force in the 3D Euclidean space, equipped with an orthonormal basis  $(\mathbf{e}_x, \mathbf{e}_y, \mathbf{e}_z)$ .

Interfacial areas and cell volumes can be easily expressed as sums on the triangles  $t$  in the mesh:

$$A_{lm} = \sum_{t \in \{lm\}} a^t, \quad V_l = \sum_{t \in l} v^t, \quad (2.16)$$

where  $a^t$  and  $v^t$  are respectively the elementary area and volume of a given triangle  $t = \{\mathbf{x}_0^t, \mathbf{x}_1^t, \mathbf{x}_2^t\}$ , which are given by

$$a^t = \frac{1}{2} |(\mathbf{x}_0^t - \mathbf{x}_2^t) \times (\mathbf{x}_1^t - \mathbf{x}_2^t)| \quad (2.17)$$

$$v^t = \frac{1}{6} \mathbf{x}_2^t \cdot (\mathbf{x}_0^t \times \mathbf{x}_1^t) \quad (2.18)$$

Their derivatives with respect to the vertex position  $\mathbf{x} = \mathbf{x}_2^t$  may be easily calculated as

$$\frac{\partial a^t}{\partial \mathbf{x}^t} = \frac{1}{2} [\mathbf{n}^t \times (\mathbf{x}_1^t - \mathbf{x}_0^t)] \quad (2.19)$$

$$\frac{\partial v^t}{\partial \mathbf{x}^t} = \frac{1}{6} \mathbf{x}_0^t \times \mathbf{x}_1^t \quad (2.20)$$

where we have defined the normal  $\mathbf{n}^t = \frac{(\mathbf{x}_0^t - \mathbf{x}_2^t) \times (\mathbf{x}_1^t - \mathbf{x}_3^t)}{2a^t}$  to the triangle  $t$ . Note that these formulae are invariant by permutation of the triplet of vertices  $\{0, 1, 2\}$ .

The force on a vertex  $\mathbf{x}$  defined in (2.15) may now be explicitly expressed as

$$\mathbf{f} = -\frac{\partial \mathcal{E}}{\partial \mathbf{x}} + \sum_{\text{cell1}} p_l \frac{\partial V_l}{\partial \mathbf{x}} \quad (2.21)$$

$$= -\sum_{\text{pair } \{lm\}} \frac{\gamma_{lm}}{2} \sum_{t \in \{lm\} | \mathbf{x} \in t} \mathbf{n}^t \times (\mathbf{x}_1^t - \mathbf{x}_0^t) + \sum_{\text{cell1}} p_l \sum_{t \in l | \mathbf{x} \in t} \frac{1}{6} \mathbf{x}_0^t \times \mathbf{x}_1^t \quad (2.22)$$

where we assumed without loss of generality that  $\mathbf{x} = \mathbf{x}_2^t$ , relying on the above invariance by permutation of derivatives formula.

**Constrained optimization: projection method** At mechanical equilibrium, all interfaces follow Laplace's law and each junction verifies Young-Dupré's equations. These equations may be equivalently expressed through a constrained optimization of the surface energy (2.13), where cell volumes are conserved. Using the Lagrangian function defined above in (2.14), optimality conditions are obtained when

$$\frac{\partial \mathcal{L}}{\partial \mathbf{x}} = -\mathbf{f}(\mathbf{x}) = \mathbf{0} \quad \forall \mathbf{x} \in \{\mathbf{x}_k\}_{k=1}^n \quad (2.23)$$

$$\frac{\partial \mathcal{L}}{\partial p} = 0 \quad \forall p \in \{p_l\}_{l=1}^N \iff V_l = V_l^0 \quad \forall l \quad (2.24)$$

To calculate the Lagrange multipliers  $p_{l=1}^N$ , which enforce the volume conservation equations (2.24), one can use a projection method. The force  $\mathbf{f}_k = \mathbf{f}(\mathbf{x}_k)$  of each vertex  $\mathbf{x}_k$  is projected onto a subspace that is orthogonal to the space of cell volumes variations

$$0 = \sum_{k=1}^n \mathbf{f}_k \cdot \frac{\partial V_l}{\partial \mathbf{x}_k} \quad \forall l \in \llbracket 1, N \rrbracket \quad (2.25)$$

This leads to a linear system of equations for  $p_l$

$$\forall l \in \llbracket 1, N \rrbracket \quad \sum_{m=1}^N p_m \sum_{k=1}^n \left( \frac{\partial V_m}{\partial \mathbf{x}_k} \cdot \frac{\partial V_l}{\partial \mathbf{x}_k} \right) = \sum_{k=1}^n \left( \frac{\partial \mathcal{E}}{\partial \mathbf{x}_k} \cdot \frac{\partial V_l}{\partial \mathbf{x}_k} \right) \quad (2.26)$$

that may be rewritten in a condensed form  $\underline{\mathbf{A}} \cdot \mathbf{p} = \mathbf{b}$ , where  $\mathbf{p} \equiv (p_1, p_2, \dots, p_N)$  is a vector of size  $N$  collecting the unknown pressures,  $\mathbf{b} \equiv \left( \sum_k \left( \frac{\partial \mathcal{E}}{\partial \mathbf{x}_k} \cdot \frac{\partial V_1}{\partial \mathbf{x}_k} \right), \sum_k \left( \frac{\partial \mathcal{E}}{\partial \mathbf{x}_k} \cdot \frac{\partial V_2}{\partial \mathbf{x}_k} \right), \dots, \sum_k \left( \frac{\partial \mathcal{E}}{\partial \mathbf{x}_k} \cdot \frac{\partial V_N}{\partial \mathbf{x}_k} \right) \right)$  is the vector of constants and  $\underline{\mathbf{A}}$  is the matrix of coefficients defined by

$$A_{lm} = \sum_k \left( \frac{\partial V_m}{\partial \mathbf{x}_k} \cdot \frac{\partial V_l}{\partial \mathbf{x}_k} \right) \quad \forall l, m \in \llbracket 1, N \rrbracket \quad (2.27)$$

which is a symmetric positive definite and therefore invertible matrix. This linear system of  $N$  equations may be solved using a Newton's method [10].

To find the mechanical equilibrium, one needs to solve the equation (2.23):  $\forall \mathbf{x}, \mathbf{f}(\mathbf{x}) = 0$ . To do so, one can use an iterative method, for instance the conjugate gradient, whereby the position  $\mathbf{x}(t)$  of each vertex at time  $t$  is updated iteratively along a new search direction  $\mathbf{D}_{t+1}$  that is conjugate to the one at previous time step  $\mathbf{D}_t$  [10].

At each iteration, the cell pressures are recalculated using the projection method.

The constrained optimization method is applied to a non-manifold multimaterial mesh. The identity of each interface separating cells  $i$  and  $j$  is tracked over its evolution by a label of integers  $(i, j)$  that is stored in each triangle of the interface. To maintain numerical precision, the triangular mesh is furthermore allowed to vary the number of vertices, edges and faces over its evolution (remeshing), and to perform topological transitions: T1 (neighbor exchange), T2 (region collapse) and merging (new contact). Note that, in contrast to classical vertex models where cell-cell boundaries are assumed to remain flat, this generic vertex model does not impose any prior constraints on cell shapes. Its precision to represent smooth and continuous interfaces is only limited by the user-defined resolution of the triangular mesh.

# Bibliography

- [1] Andrew R Harris, Loic Peter, Julien Bellis, Buzz Baum, Alexandre J Kabla, and Guillaume T Charras. Characterizing the mechanics of cultured cell monolayers. *Proceedings of the National Academy of Sciences*, 109(41):16449–16454, 2012.
- [2] Matthias Merkel, Raphaël Etournay, Marko Popović, Guillaume Salbreux, Suzanne Eaton, and Frank Jülicher. Triangles bridge the scales: Quantifying cellular contributions to tissue deformation. *Physical Review E*, 95(3):032401, 2017.
- [3] S Ishihara, K Sugimura, SJ Cox, Isabelle Bonnet, Y Bellaïche, and F Graner. Comparative study of non-invasive force and stress inference methods in tissue. *The European Physical Journal E*, 36(4):1–13, 2013.
- [4] Reza Farhadifar, Jens-Christian Röper, Benoit Aigouy, Suzanne Eaton, and Frank Jülicher. The influence of cell mechanics, cell-cell interactions, and proliferation on epithelial packing. *Current Biology*, 17(24):2095–2104, 2007.
- [5] Douglas B Staple, Reza Farhadifar, J-C Röper, Benoit Aigouy, Suzanne Eaton, and Frank Jülicher. Mechanics and remodelling of cell packings in epithelia. *The European Physical Journal E*, 33(2):117–127, 2010.
- [6] Edouard Hannezo, Jacques Prost, and Jean-Francois Joanny. Theory of epithelial sheet morphology in three dimensions. *Proceedings of the National Academy of Sciences*, 111(1):27–32, 2014.
- [7] Hisao Honda, Masaharu Tanemura, and Tatsuzo Nagai. A three-dimensional vertex dynamics cell model of space-filling polyhedra simulating cell behavior in a cell aggregate. *Journal of theoretical biology*, 226(4):439–453, 2004.
- [8] Satoru Okuda, Takashi Miura, Yasuhiro Inoue, Taiji Adachi, and Mototsugu Eiraku. Combining turing and 3d vertex models reproduces autonomous multicellular morphogenesis with undulation, tubulation, and branching. *Scientific reports*, 8(1):1–15, 2018.
- [9] Jean-Léon Maître, Hervé Turlier, Rukshala Illukkumbura, Björn Eismann, Ritsuya Niwayama, François Nédélec, and Takashi Hiiragi. Asymmetric division of contractile domains couples cell positioning and fate specification. *Nature*, 536(7616):344–348, 2016.
- [10] Jorge Nocedal and Stephen J Wright. Conjugate gradient methods. *Numerical optimization*, pages 101–134, 2006.